metals

MDPI

Article

Strengthening Mechanisms of Aluminum Matrix Nanocomposites Reinforced with CNTs Produced by Powder Metallurgy

Íris Carneiro [1,2], José Valdemar Fernandes [3] and Sónia Simões [1,2,*]

[1] DEMM, Department of Metallurgical and Materials Engineering, University of Porto, Rua Doutor Roberto Frias, 4200-465 Porto, Portugal; up201207199@fe.up.pt
[2] LAETA/INEGI, Institute of Science and Innovation in Mechanical and Industrial Engineering, Rua Doutor Roberto Frias, 4200-465 Porto, Portugal
[3] CEMMPRE, Centre for Mechanical Engineering, Materials and Processes, Department of Mechanical Engineering, University of Coimbra, Rua Luís Reis Santos, Pinhal de Marrocos, 3030-788 Coimbra, Portugal; valdemar.fernandes@dem.uc.pt
* Correspondence: ssimoes@fe.up.pt; Tel.: +351-220413113

Abstract: The present work aims to investigate the strengthening mechanisms in aluminum matrix nanocomposites reinforced by carbon nanotubes (CNTs). A classical powder metallurgy route produced Al-CNT nanocomposites using ultrasonication and ball milling as dispersion/mixture techniques. The microstructural characterization is crucial for this study to reach the objective, being performed mainly by electron backscattered diffraction (EBSD), transmission electron microscopy (TEM), and high-resolution TEM (HRTEM). Uniform dispersion without damaging the CNTs structure is the key for the nanocomposite by powder metallurgy production process. The reinforcement effect occurs due to several strengthening mechanisms that act simultaneously. For the Al-CNT nanocomposites produced by ultrasonication as a dispersion/mixture technique, the observed improvement in the mechanical properties of nanocomposites can be attributed to the load transfer from the matrix to the CNTs. The strain hardening and the second-phase hardening can also have a small contribution to the strengthening of the nanocomposites.

Keywords: strengthening mechanisms; metal matrix nanocomposites; powder metallurgy; load transfer; second-phase particles; strain hardening

Citation: Carneiro, Í.; Fernandes, J.V.; Simões, S. Strengthening Mechanisms of Aluminum Matrix Nanocomposites Reinforced with CNTs Produced by Powder Metallurgy. *Metals* **2021**, *11*, 1711. https://doi.org/10.3390/met11111711

Academic Editors: Marta Cabeza Simó and Mieczyslaw Jurczyk

Received: 24 September 2021
Accepted: 23 October 2021
Published: 27 October 2021

1. Introduction

Nanocomposites are a focus in materials science and engineering due to their improved properties compared to microscale-reinforced composites [1,2]. In a metallic matrix, the enhancement of a targeted property depends on several factors, including the type of reinforcement, size, amount, degree of dispersion, and the possible interaction between the matrix and an eventual second phase [3,4]. One of the most remarkable reinforcing materials is carbon nanotubes (CNTs), which have received significant attention due to their extraordinary physical and mechanical properties, proving to be the ideal reinforcement for metal matrix nanocomposites (MMNCs) [2,4]. MMNCs, reinforced by CNTs, have been studied using matrices of pure metals, for example, Ni [5–11], Cu [12–17], Ti [18–23], Mg [24–29], and, more broadly, Al [30–40]. Gradually, research began to analyze the effect of CNTs on pure metals and their alloys [24,41–44].

The strengthening mechanisms remain a widely investigated topic, as their identification and understanding are crucial to optimizing nanocomposites' implementation. Although the load transfer from the matrix to the reinforcement [9,24,25] is the most widely reported, others have also been identified [19–26] as grain refinement, Orowan hardening

[9,26–30], solid solution strengthening [31], second-phase hardening, and strain hardening (increase in dislocation density) [26,27,32,33,45].

Xu et al. [36] produced aluminum nanocomposites with 2 wt. % CNTs and observed an increase in strength of 102% compared to the unreinforced aluminum produced under the same conditions. This improvement was attributed to several strengthening mechanisms acting simultaneously in the nanocomposite: a significant grain refinement, the formation of second-phase particles of Al_4C_3, the increase in dislocation density, and the Orowan mechanism associated with the presence of CNTs and those second-phase particles.

Several strengthening mechanisms were also identified by Chen et al. [46] in aluminum nanocomposites, which contributed to different extents. The authors observed an increase in the tensile strength of Al-CNTs that correlated to the grain refinement, load transfer, thermal mismatch, and Orowan mechanism.

Han et al. [47] produced aluminum composites reinforced by graphene nanoplates and observed improved yield and ultimate tensile strength combined with good ductility. The authors also investigated the strengthening mechanisms and observed that the graphene nanoparticles are an obstacle to the dislocations and grain boundary mobility, contributing to increased dislocation density and inhibiting grain growth. In addition to graphene, this effect was also mentioned for CNTs in other works, where the interfacial nanoparticles can substantially improve the load transfer mechanism [48].

Chen et al. [49] studied the load transfer mechanism in Al-CNT nanocomposites, with 0.6 wt % reinforcement, and the influence of introducing Al_2O_3 interfacial nanoparticles. The authors observed that the CNTs act as bridges between points in the matrix, preventing crack growth. With the application of higher loads, the tensile strain increases, and the CNTs acting as bridges fracture the outer walls, while the inner parts are undamaged and in a columnar shape. The presence of Al_2O_3 nanoparticles changes the interface morphology, making it tortuous and advantageous to anchor the CNTs and resist their pull-out. Therefore, their presence is highly effective for the load-transfer mechanism, leading to the CNTs fracture and no pull-out during tensile loading.

Chen et al. [50] studied the interaction between CNTs and aluminum in nanocomposites produced by spark plasma sintering (SPS). By in situ transmission electron microscopy (TEM) observations, the authors have seen that dislocations are pinned by CNTs, restricting their movement. Due to the accumulation of pinned dislocations, low-angle boundaries form, surrounding the CNTs. The overall fraction of low-angle boundaries (associated with the increase in dislocation density) is more significant for nanocomposites than unreinforced aluminum.

Therefore, as in previous works [5,45], it was once again clear that the presence of reinforcement in Ni-CNT nanocomposites has a considerable influence on the dislocation and grain boundaries behaviors, constituting obstacles to their motion. The reinforcement prevents eliminating the effects of plastic deformation during processing, making recovery and recrystallization processes more difficult. However, it is still unclear whether this occurs to the same extent in all nanocomposite matrices reinforced with CNTs.

In this context, this work aims to identify and understand the strengthening mechanisms occurring in aluminum matrix nanocomposites. To achieve this objective, the produced nanocomposites were characterized by scanning electron microscopy (SEM), electron backscatter diffraction (EBSD), and high-resolution transmission electron microscopy (HRTEM).

2. Materials and Methods

A traditional powder metallurgy route performed the production of Al-CNT (1.00 vol.%) nanocomposites. Aluminum powders and multi-walled carbon nanotubes (MWCNTs) were used. The aluminum powders, 99.5% pure, were supplied by Goodfellow Cambridge Ltd. (Huntingdon, UK), while the MWCNTs were provided by Fibermax Nanocomposites Ltd. (London, UK). CNTs functionalized (NTX5 (Nanothinx S.A., Patras, Greece)) were also used to produce the nanocomposites.

Al and MWCNTs (functionalized and not functionalized) were fully characterized in previous works [30,32,51,52], including the size and respective distribution of aluminum powder particles, as received and after dispersion, as well as the morphology of MWCNTs, which can influence the result.

To successfully produce these types of nanocomposites and assure the efficiency of the strengthening mechanisms, it is crucial to obtain a uniform MWCNTs dispersion in the aluminum matrix. In this sense, it is essential to carefully choose the dispersion/mixing methods and conditions in the production route to obtain the expected result. Ultrasonication and its combination with ball milling were the mixture and dispersion techniques performed. The ultrasonic technique was used for the simultaneous dispersion and mixing of the MWCNTs with Al powders, using the best conditions as reported in previous work [5,30,45]; that is, this method was applied simultaneously to Al and CNTs powders in isopropanol for 15 min. The ultrasonic method is used for short periods under the same conditions to untangle some CNT clusters in a second dispersion route. After that, the dispersion and mixture of Al powder and the untangled MWCNTs were conducted by ball milling, for 360 min, with 150 rpm and a ball-to-powder ratio of 20:1. The mixtures were pressed at 300 MPa and sintered at 640 °C for 90 and 120 min under a vacuum at 10^{-2} Pa. Heat treatments were also conducted at 480 °C for 90 min. Figure 1 shows a summary of the production conditions of the nanocomposites and the samples without reinforcement.

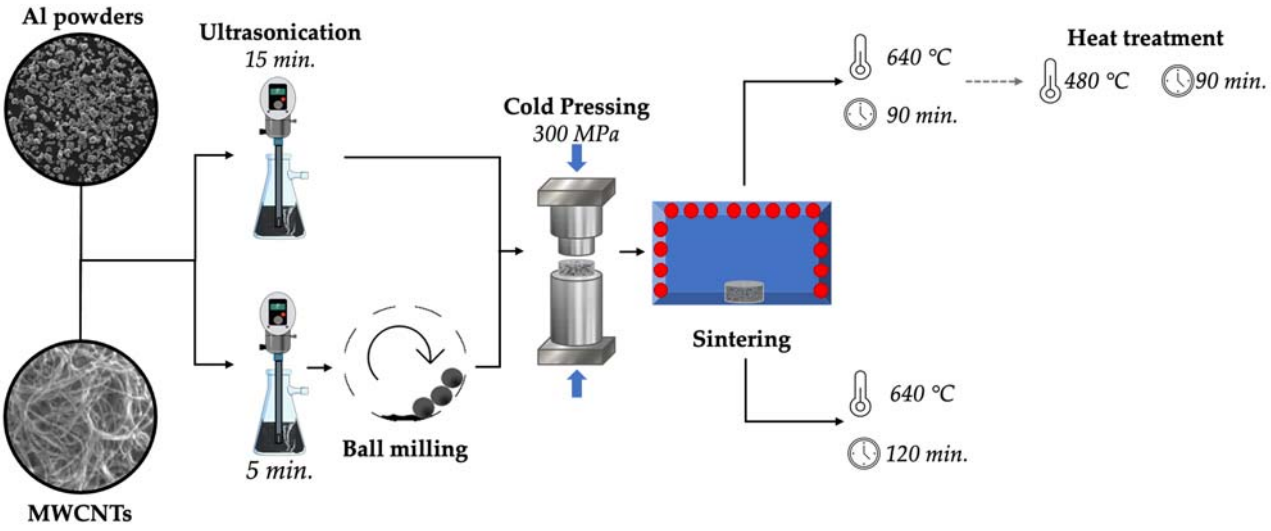

Figure 1. Scheme of the production and heat-treatment conditions of the Al and nanocomposite samples.

Optical microscopy (OM) and the image analysis software was used to overview all the produced samples and quantify the pores and agglomerates present in each one. For this, a DM 4000 M optical microscope equipped with a Leica DFC 420 camera (Leica Microsystems, Wetzlar, Germany) and the Leica Application Suite software (Leica Microsystems, Wetzlar, Germany) were used for the image analysis. The average grain value was obtained by measuring up to 500 grains per sample. Evaluating the number and average diameter of the CNT agglomerates used five fields of 489 × 653 μm² of OM imagens.

EBSD is a promising characterization technique with great potential that allows obtaining a wide variety of results to study in detail the nanocomposites microstructures. Therefore, the samples were analyzed by high-resolution SEM (Thermo Fisher Scientific QUANTA 400 FEG SEM, Thermo Fisher Scientific, Hillsboro, OR, USA), which is coupled to an EBSD detector TSL-EDAX EBSD Unit (EDAX Inc. (Ametek), Mahwah, NJ, USA). The raw data obtained are submitted to a dilatation routine clean-up. A grain tolerance angle of 15° and 2 points as minimum grain size is determined, which is crucial for preventing doubtful results. The cleaned data are used to elaborate the wide range of maps and

graphs with TSL OIM Analysis 5.2. The overall EBSD maps—inverse pole figures (IPFs) and grain orientation spread (GOS)—were obtained under conditions similar to those described in previous work [45].

Along with this, the grain average misorientation (GAM) maps were used to separate the grains into different categories (recrystallized, recovered, deformed). Using the same software, pole figures (PF) were also drawn to understand preferential crystallographic orientations and even the presence of sharp textures. The ATEX software was used, similarly to previous work [53], to elaborate maps and estimate the geometrically necessary dislocations (GNDs) density [54].

The formation of second-phase particles was analyzed by X-ray diffraction (XRD), with the MPD Panalytical X'Pert Pro (Malvern Panalytical Ltd., Malvern, UK) instrument, CuKα radiation, and diffraction patterns collected from 20° to 90° (2θ) in a θ–2θ Bragg-Brentano mode.

High-resolution TEM was very advantageous for the in-depth study of the bonding of CNTs to the metal matrix, the formation of second-phase particles resulting from the reaction between the CNTs and matrix, and the presence of dislocations and dislocations cells. A high-resolution TEM (HRTEM) (Thermo Fisher Scientific, Hillsboro, OR, USA) was used for this purpose.

Mechanical characterization was conducted to comprehend the effect of the CNTs on reinforced Al. In this sense, the samples were submitted to Vickers microhardness tests, which were performed using a Duramin-1 durometer (Duramin-1; Struers A/S, Ballerup, Denmark) and used for approximately 12 indentations in each sample, with a load of 98 mN. The tensile tests were performed at an initial strain rate of about 8×10^{-3} s^{-1}; three specimens were tested for each condition. The geometry of the tensile specimens is described elsewhere [51].

3. Results and Discussion

Figure 2 shows the optical microscopy (OM) images of the nanocomposite produced by ultrasonication or ball milling as dispersion/mixture techniques, using CNTs functionalized or non-functionalized, and during different sintering times (90 and 120 min). All nanocomposites exhibit a microstructure consisting of equiaxed aluminum grains with pores and CNT agglomerates mainly in grain boundaries, which are not distinguishable by OM (dark phase). With enhanced detail, Figure 3 shows a scanning electron microscopy (SEM) image of the nanocomposite produced using ultrasonication, confirming the presence of CNTs in the pores and grain boundaries of the Al matrix. The presence of pores characterizes the samples produced by powder metallurgy; nevertheless, it is not guaranteed that the CNTs fill all pores.

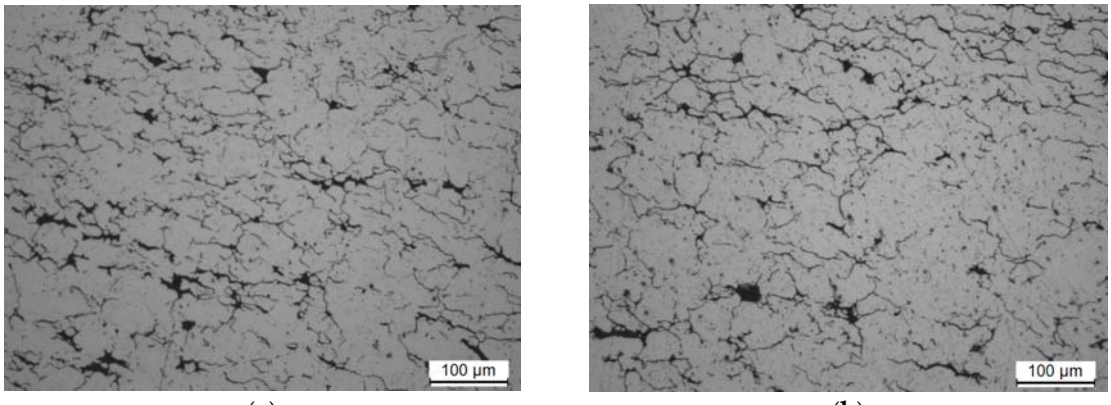

(**a**) (**b**)

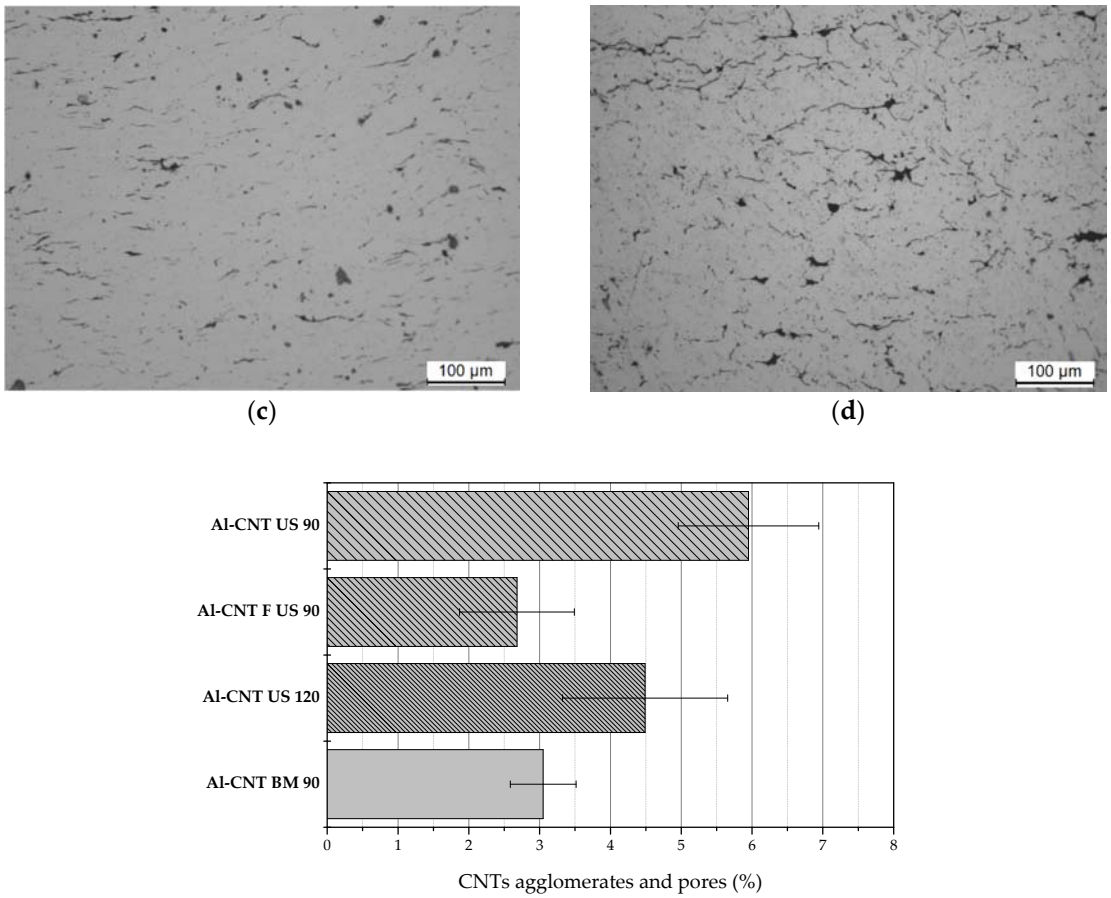

Figure 2. Optical microscopy (OM) images of Al-CNTs produced with non-functionalized CNTs (**a**–**c**) by (**a**) ultrasonication and sintering during 90 min (Al-CNT US 90), (**b**) ultrasonication and sintering during 120 min (Al-CNT US 120), (**c**) ball milling and sintering during 90 min (Al-CNT BM 90), (**d**) produced with functionalized CNTs by ultrasonication and sintering during 90 min. (Al-CNT US F 90) and (**e**) Percentage of CNT agglomerates and pores of the nanocomposites in the OM figures.

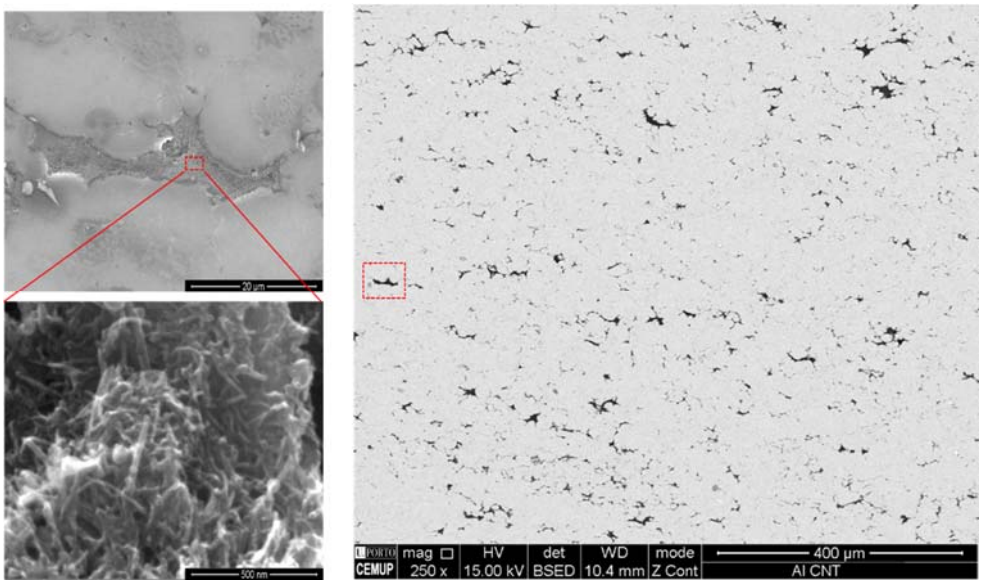

Figure 3. Scanning electron microscopy (SEM) images of Al-CNTs produced by ultrasonication and sintering during 120 min.

Dispersion/mixture techniques, sintering time, and the use of CNTs functionalized treatment strongly influence the dispersion of the CNTs. The nanocomposites produced by ball milling and ultrasonication with functionalized CNTs exhibit a smaller amount (2.68% and 3.05%, respectively) of CNT agglomerates. This can be an indication of a uniform dispersion obtained for these nanocomposites. The nanocomposites produced by ultrasonication revealed a percentage of CNT agglomerates of 5.95% and a maximum size of 78 μm [30]. Increasing the sintering time promotes the decrease of the amount and size of CNT agglomerates to 4.49% and 61.4 μm, respectively.

Figure 4 shows the influence of dispersion/mixture processes, sintering time, and functionalization of the CNTs on the mechanical properties of nanocomposites. This evolution shows an increase in the hardness and ultimate tensile strength and a decrease in the nanocomposites' elongation concerning the Al matrix's same properties produced under the same conditions (yield strength of 23 MPa, an ultimate tensile strength of 66 MPa, an elongation of 28%, and 34 HV 0.1 [51]). Although the properties reported for Al-CNT nanocomposites depend significantly on the type of dispersion/mixing and processing methods, these properties are according to the expected ones [31,34–39].

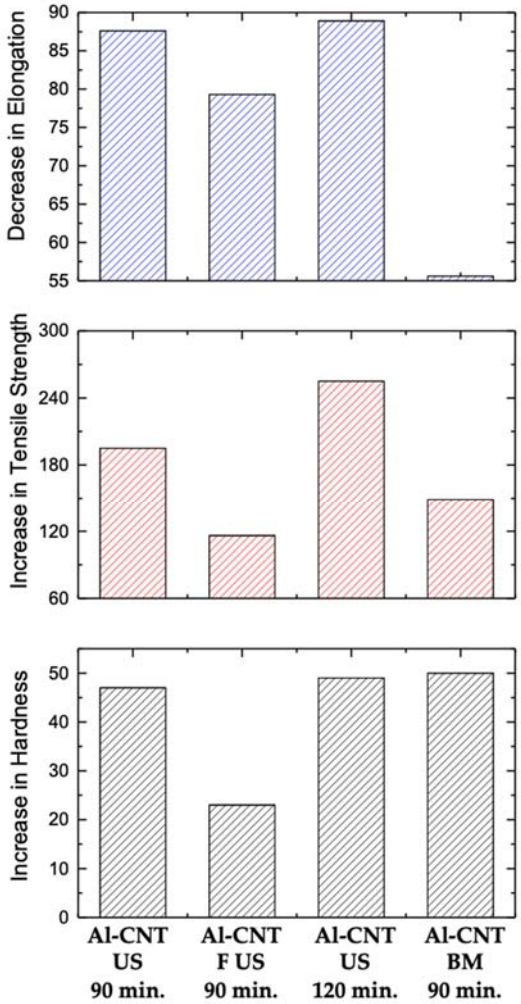

Figure 4. Percentage of increase in hardness (HV 0.01) and ultimate tensile strength (MPa) and decrease in elongation (%) for the nanocomposites, concerning the same properties for the Al matrix produced under the same conditions. The designations are the same as in Figure 2.

All nanocomposites revealed a higher hardness and ultimate tensile strength than Al produced in the same conditions, corroborating the strengthening effect of introducing

the CNTs into the metal matrix. Furthermore, these values also confirm the quality of the CNTs dispersion.

Although having a more significant amount of CNT clusters, the nanocomposites produced with ultrasonication as the dispersion/mixture process present a greater increase in hardness (from 34 to 50 HV0.01) and ultimate tensile strength (from 66 to 196 MPa for 90 min of sintering and from 72 to 257 MPa, increasing the sintering for 120 min), revealing the most favorable conditions to make these nanocomposites.

While the Al-CNT nanocomposites produced with functionalized CNTs present a better dispersion, the structural damage caused by the functionalization treatment affects the CNTs' strengthening potential. The increase in hardness was only from 34 to 42 HV0.01, and the increase in ultimate tensile strength was from 66 to 143 MPa. These results were similar to those observed for the Ni-CNTs nanocomposites in our previous work [52] and to the work of Xu et al. [36]. It was clear that the functionalization treatment of CNTs and ball milling promotes defects in the structure, which affected the hardness value and strength obtained for the nanocomposites.

Nanocomposites produced by ball milling also improve the mechanical properties, but the increase is slightly lower than expected, especially the ultimate tensile strength (from 87 to 216 MPa). The microstructural characterization revealed a more uniform CNTs dispersion with smaller-sized agglomerates, and therefore, a more significant improvement in mechanical properties than ultrasonication was expected. The reason for this is the damage suffered by CNTs during the functionalization process. The ball milling method promotes damage to the structure of CNTs, which was proved by HRTEM and Raman spectroscopy in previous work [32], reducing their potential for strengthening. For effective strengthening, there must be not only a uniform dispersion of the CNTs strongly bonded to the matrix but also a preserved CNTs structure without damage.

Since the Al-CNT nanocomposites produced by ball milling as the dispersion/mixture process or using functionalized CNTs reveal an increase in the mechanical properties that were lower than expected, the present work focuses on the study of the strengthening mechanisms mainly in the samples produced by ultrasonication.

The nanocomposite fracture surfaces were analyzed to investigate the load transfer mechanism. In this analysis, fractured and pulled-out CNTs were present in all nanocomposites. Figure 5 shows illustrative SEM images of the fracture surface of the Al-CNTs produced by ultrasonication.

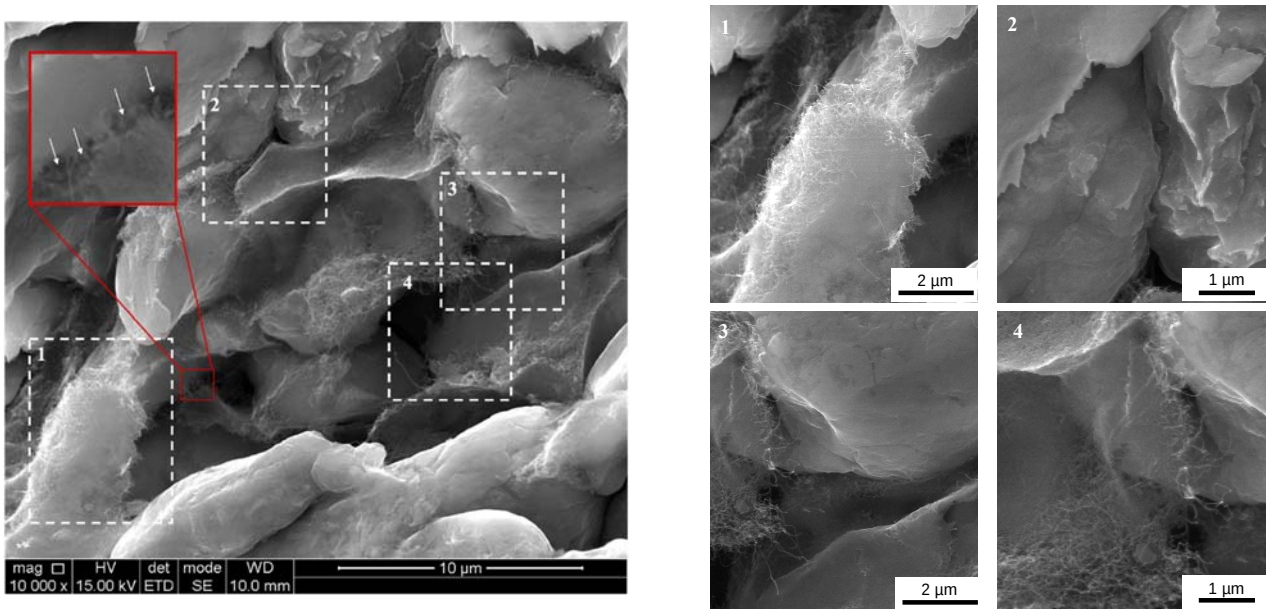

(**a**) (**b**)

Figure 5. SEM images of the fracture surface of nanocomposites produced using ultrasonication: (**a**) lower magnification and (**b**) higher magnification of the regions marked in (**a**) where pulled-out and ruptured CNTs can be observed.

High-magnification SEM images show that ruptured or pulled-out CNTs can be identified. These observations prove that one of the strengthening mechanisms present is load transfer. When the matrix undergoes plastic deformation, nucleation and cracks propagation occur. The presence of CNTs will allow them to act as bridges and restrain the crack growth.

The load transfer is one of the mechanisms that most contribute to the strengthening effect in nanocomposites reinforced with CNTs [9,55,56]. However, other mechanisms are simultaneously present, playing a role in increasing the mechanical properties of nanocomposites. In a previous study [53], the strengthening mechanisms occurring in nickel nanocomposites reinforced by CNTs were carefully investigated. Load transfer and increased dislocation density seem to strongly affect the properties and microstructure of the nanocomposite. The grain refinement and the presence of second phase particles have a small contribution to the strengthening of this nanocomposite.

Microstructural features such as grain size and orientation, increased dislocation density, and the formation of second-phase particles can also contribute to the nanocomposites strengthening [6,10,23,36,57]. The final microstructural features are perceived by inverse pole figures (IPF) maps, image quality (IQ) maps with delineated high- and low-angle boundaries, grain orientation spread (GOS) maps, and pole figures (PF) for the nanocomposites produced by ultrasonication, which can be observed in Figure 6.

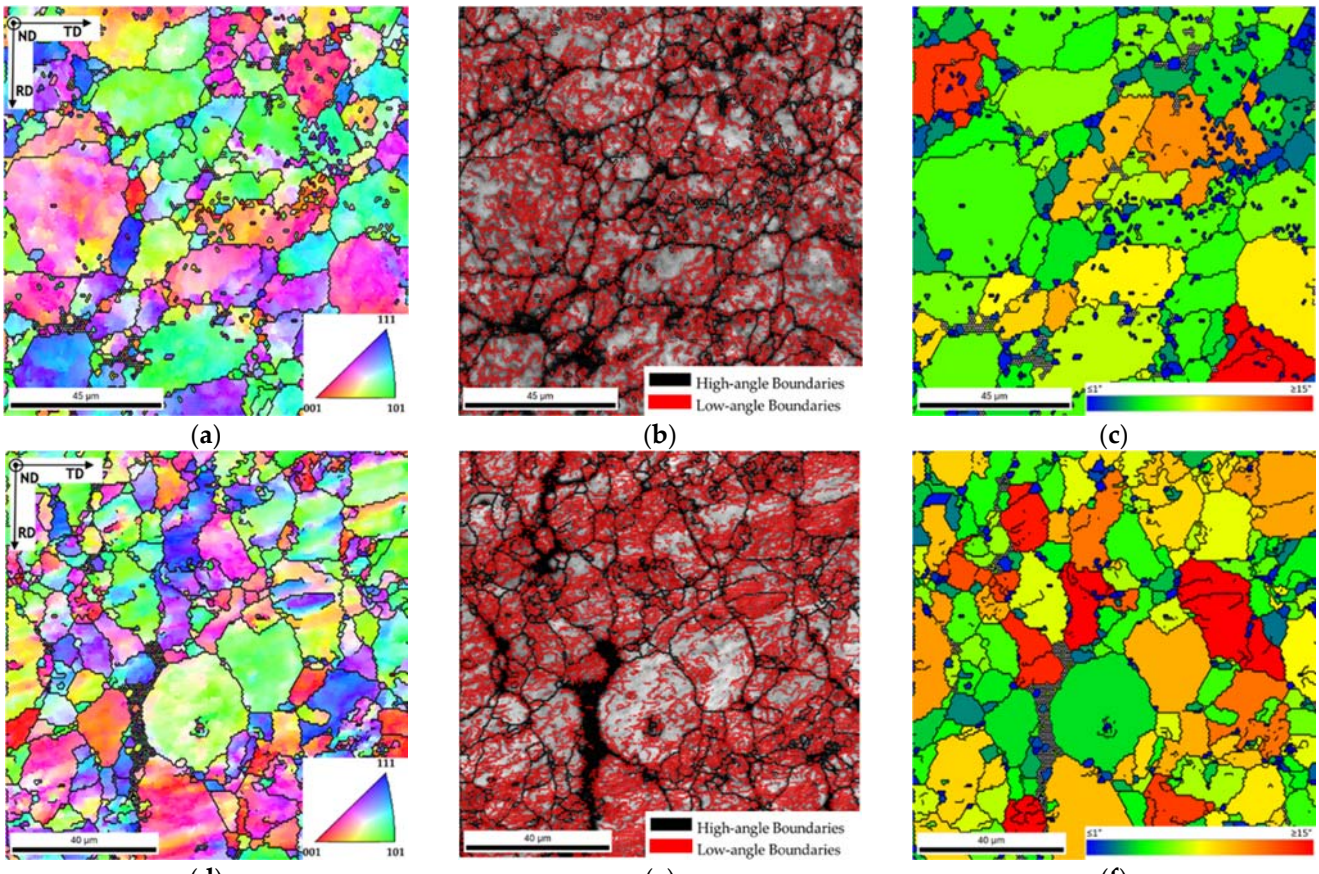

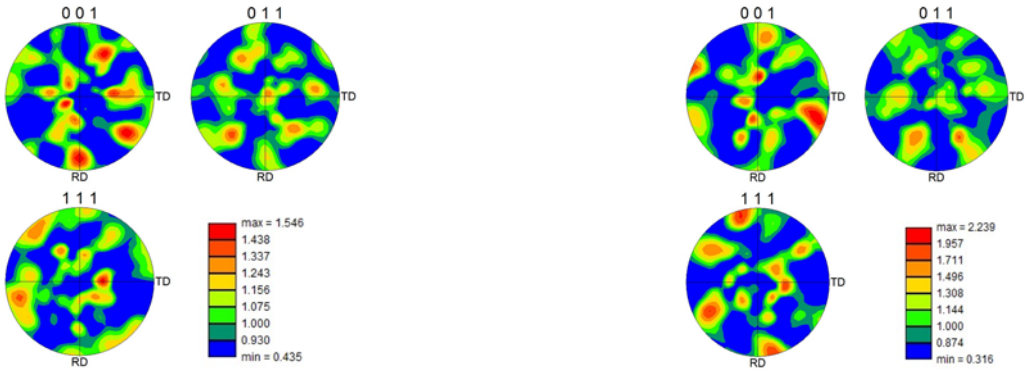

(**g**) (**h**)

Figure 6. IPF maps, IQ maps with high- and low-angle boundaries delineated, GOS maps, and PF of (**a**–**c**,**g**) Al and (**d**–**f**,**h**) Al-CNTs produced by ultrasonication.

Figure 6 reveals that similar grain sizes, low-angle boundary densities, and grain orientations are observed for Al and Al-CNTs produced by ultrasonication. The GOS maps show the main difference between these samples. Although not very noticeable, the nanocomposites have a lower percentage of fully recrystallized grains (in blue), along with a high content of slightly deformed grains (represented by green) and some significantly deformed grains (orange and red). These results show that CNTs affect the extension of the recovery and recrystallization processes of the Al matrix during the sintering. In the case of Ni-CNT composites produced under similar conditions [45,53], more significant differences were observed in the texture and density of low-angle boundaries induced by the introduction of CNTs.

To further investigate the effect of the CNTs on the recovery and recrystallization processes, a heat treatment was conducted at 480 °C for 90 min under vacuum. Figure 7 shows the grain size, GOS, and GAM maps for the Al and Al-CNTs produced using ultrasonication, sintered for 90 min, and then heat-treated. Based on these results, recrystallized grains are observed for the heat-treated Al samples. Moreover, the grain size is smaller for the Al than Al-CNT samples due to the recovery and recrystallization process. The nanocomposites show a lower density of small, recrystallized grains and the presence of deformed grains.

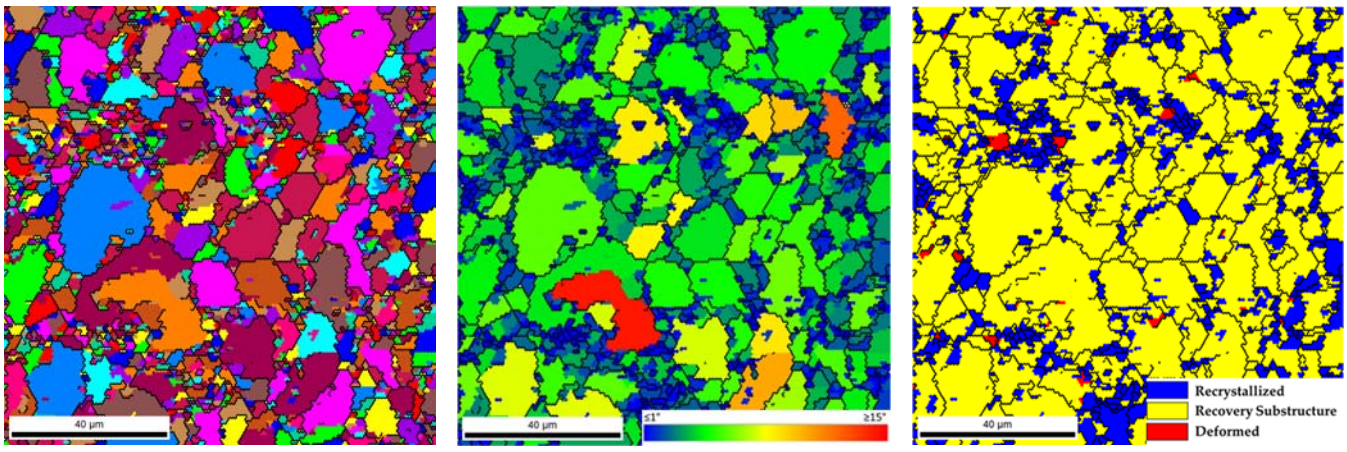

(**a**) (**b**) (**c**)

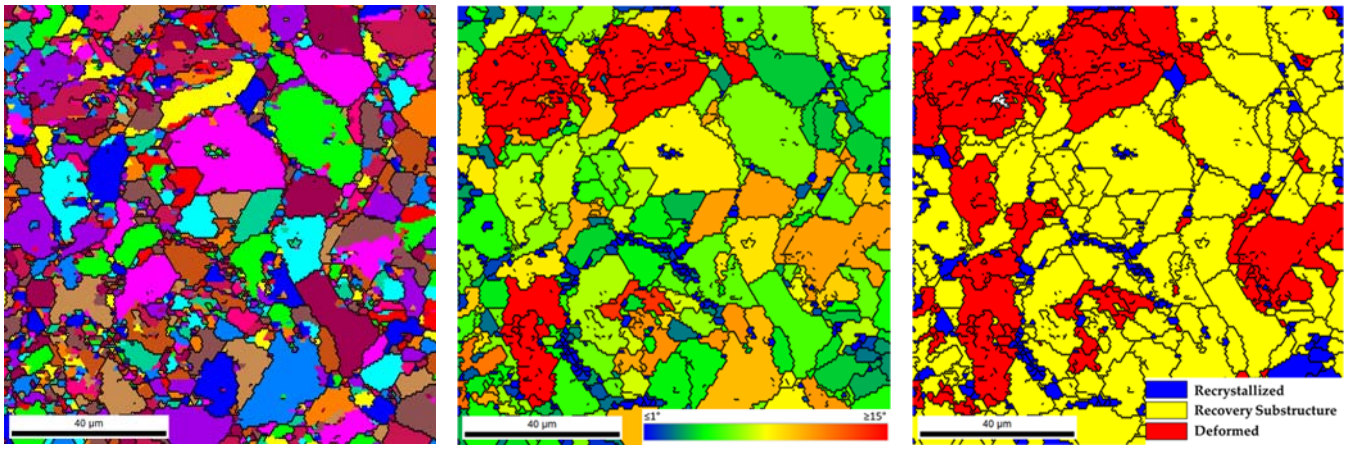

(**d**) (**e**) (**f**)

Figure 7. Grain size, GOS, and GAM maps of (**a**–**c**) Al and (**d**–**f**) Al-CNTs produced by ultrasonication sintered during 90 min and heat-treated at 480 °C during 90 min.

The nanocomposites reveal a slight increase in local misorientation spread than the Al samples produced under the same conditions, proving some effect of the CNTs on the dislocation arrangement during the sintering. However, the impact is not as significant as that observed for Ni-CNT nanocomposites [53].

Figure 8, using high magnifications, exhibit better a slight difference between the samples. This figure shows the IPF and IQ maps with high- and low-angle grain boundaries and GND estimated density maps for the Al and Al-CNT samples produced by ultrasonication. For the nanocomposites, a slightly higher density of low-angle grain boundaries was observed associated with a somewhat higher GND density (4.99×10^{14} m^{-2} and 5.39×10^{14} m^{-2}, respectively). The increase in the dislocation density can be attributed to the pinning effect of the CNTs, as mentioned by Chen et al. [50], or even to the impact of thermal mismatch strain [46].

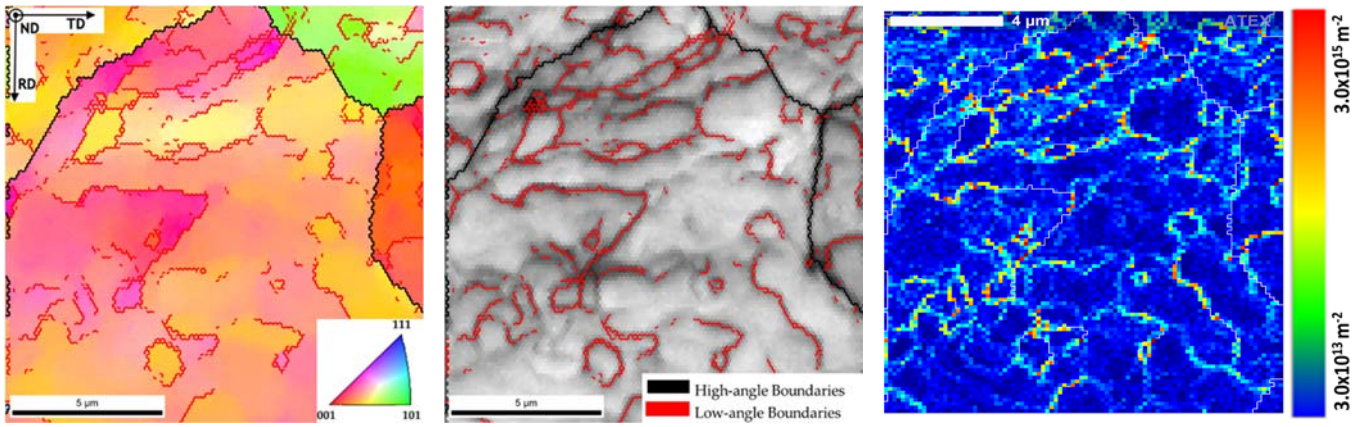

(**a**) (**b**) (**c**)

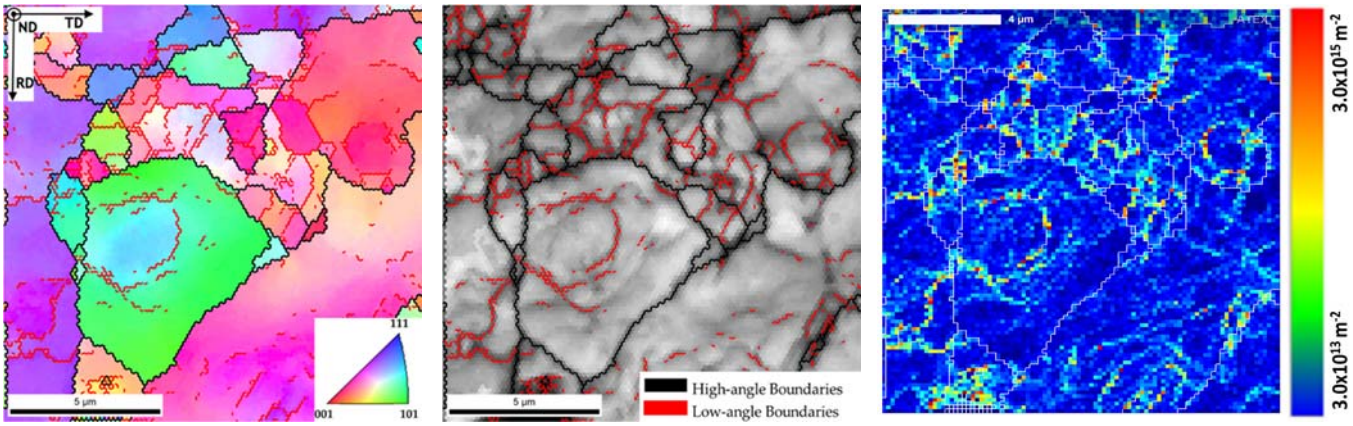

Figure 8. IPF, IQ maps with high- (black) and low-angle boundaries (red) delineated, and geometrically necessary dislocations (GNDs) density maps of (**a**–**c**) Al and (**d**–**f**) Al-CNTs as produced by ultrasonication sintered during 90 min.

The TEM and HRTEM images were also used to characterize, with more detail, some of the microstructural features of the nanocomposites. Figure 9 shows images of Al and Al-CNT as produced by ultrasonication and heat-treated. For the nanocomposites, there is a higher density of dislocations. This confirms that the introduction of CNTs into the Al matrix affects the dislocation motion and rearrangement during the sintering. In the Al samples, the microstructure presents equiaxed grains. Although the CNT clusters are observed by OM and SEM images, CNTs are also embedded in the matrix. These CNTs strongly bound to the metallic matrix are essential for the strengthening effect.

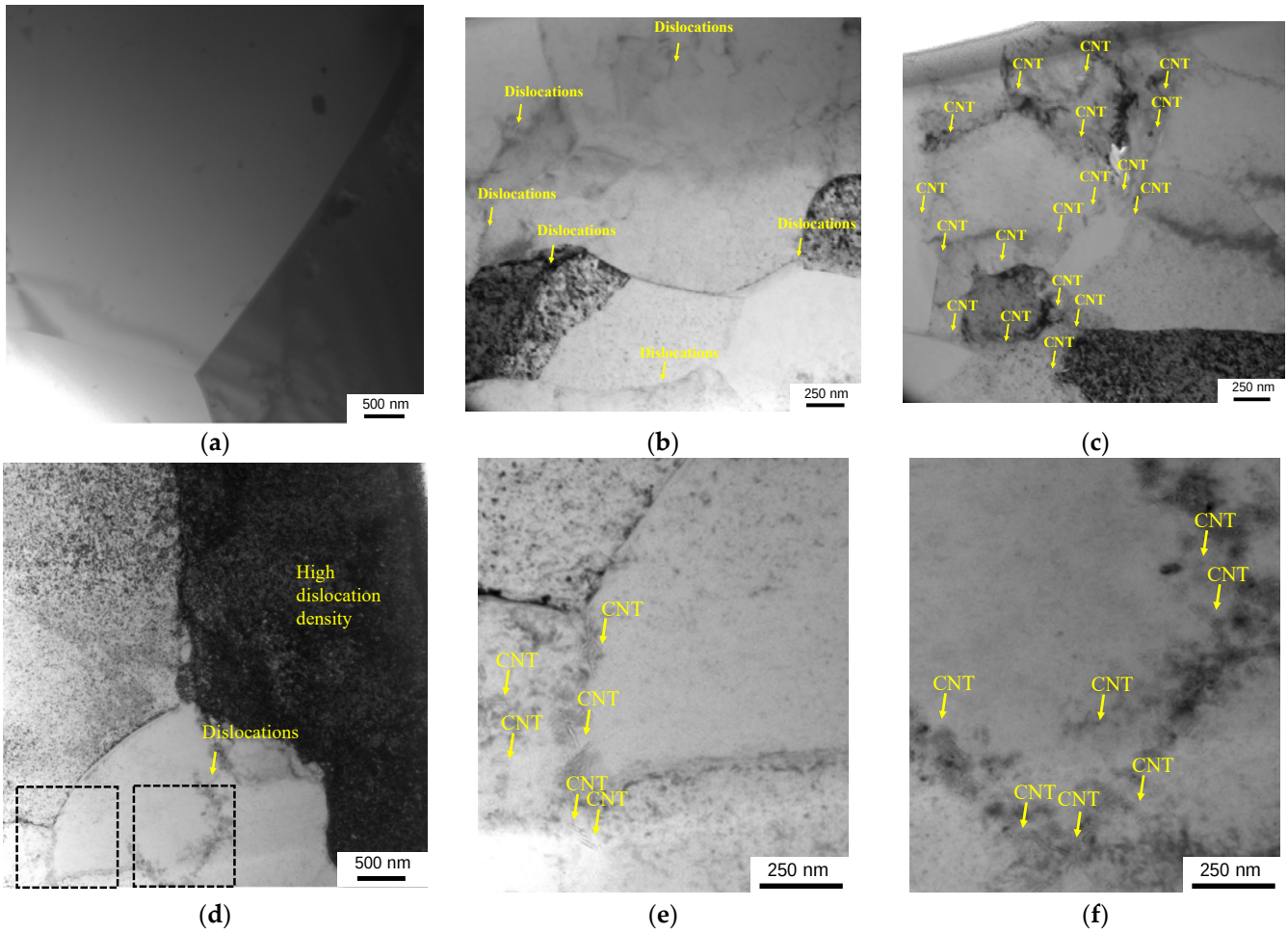

Figure 9. TEM images of (**a**) Al, (**b**,**c**) Al-CNTs nanocomposite as produced by ultrasonication sintered during 90 min and (**d**) Al-CNTs heat-treated, and (**e**,**f**) high magnification of regions marked in (**d**).

TEM analysis shows the presence of the Al_4C_3 phase, as shown in Figure 10. In these images, it is possible to see the presence of these second-phase particles, especially near the CNTs. Even in small quantities, these particles can contribute to the strengthening effect observed in the nanocomposites, improving the bonding between the CNTs and the matrix [37,58–60] as well as acting as obstacles to the motion of dislocation [36,60] and grain boundaries [36], promoting grain refining.

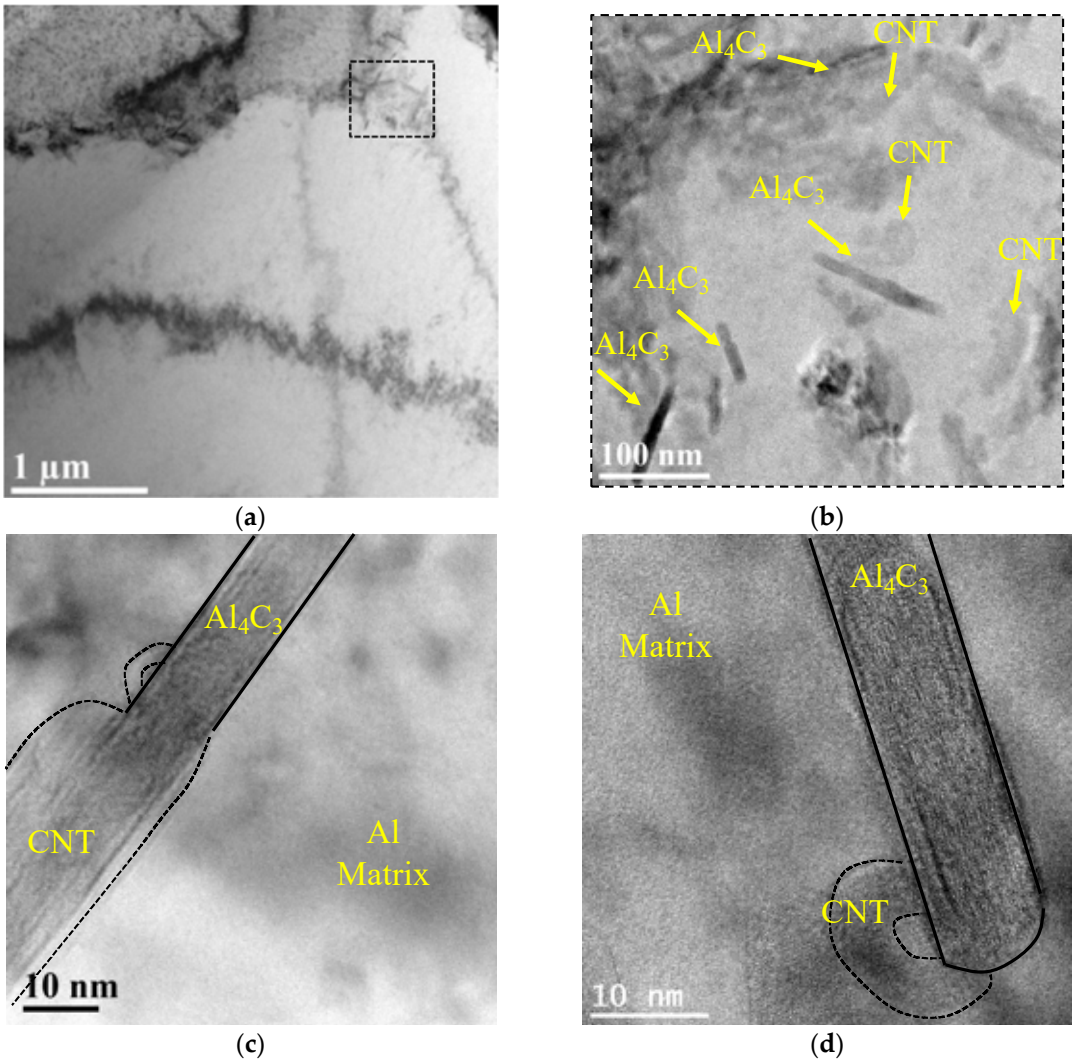

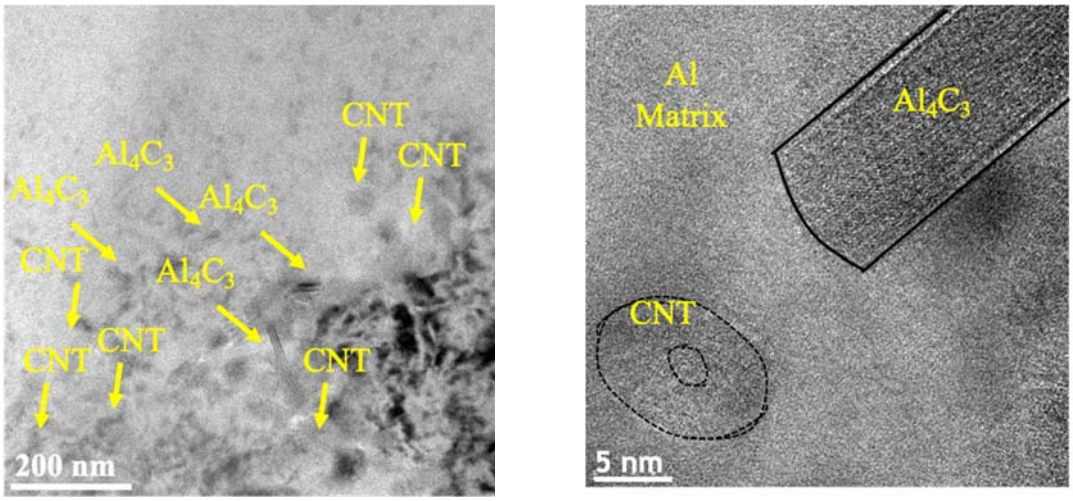

(**e**) (**f**)

Figure 10. TEM images of Al-CNT nanocomposites produced by ultrasonication for 90 min, showing (**a**,**b**) the presence of the Al_4C_3 phase (**b**) magnification of the marked zone in (**a**); (**c**) partial transformation of Al_4C_3 particles and carbon nanotubes, (**d**) full transformation of an Al_4C_3 particle being surrounded by a carbon nanotube, (**e**,**f**) TEM image of the heat-treated nanocomposite showing the presence of Al_4C_3 and CNTs and HRTEM.

The nanocomposite application may be compromised if, during the application, reaction or damage to the reinforcement occurs due to the service temperature. In this sense, the observations in TEM and HRTEM were made to evaluate the reaction and structure of the CNTs. The heat treatment of the nanocomposites at 480 °C did not significantly change the formation of Al_4C_3 particles or even in the damage of CNTs. Figure 10e,f shows the results of the TEM images for the heat-treated nanocomposites samples. The nanocomposites with and without heat treatment show similar results regarding Al_4C_3 particles close to the CNTs. The heat treatment did not significantly affect the reaction between the CNTs and the matrix.

The formation of this second phase in Al-CNT nanocomposites was also observed in previous work [32,51] and by other authors [58,59]. Note that Yu et al. [37] observed, using HRTEM, the formation of an Al_4C_3 phase closely connected to the open end of a CNT in a nanocomposite with an Al-Mg alloy as the matrix.

These aluminum carbides are formed by the total or partial chemical reaction between the CNTs and the matrix, as schematically illustrated in Figure 11. The partial reaction results in interfacial Al_4C_3 particles between the matrix and the reinforcement, improving their bonding and contributing to the efficiency of the load transfer mechanism. When the reaction is total, the full transformation into individual Al_4C_3 particles strengthens the nanocomposite, acting as a barrier to the dislocation motion and rearrangement and grain boundaries, preventing grain growth.

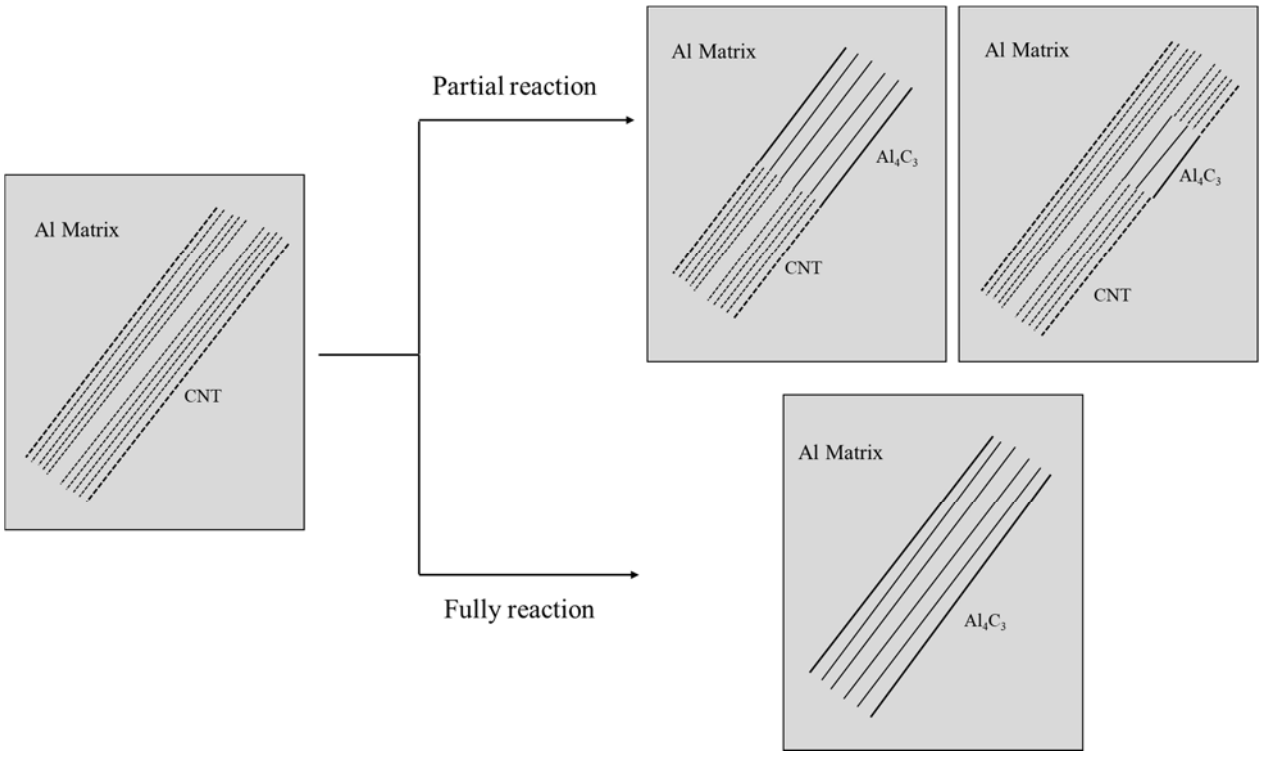

Figure 11. Schematic drawing of different reactions between the CNT and matrix forming the Al_4C_3 phase.

Some investigations evaluated the effect of the Al_4C_3 formation on the improvement also of the load transfer mechanism. Kwon et al. [48] observed two types of Al_4C_3 particles in Al-CNT nanocomposites (1.00 vol % CNTs), which they defined as dumbbell and tube types. Dumbbell-shaped ones are derived from the CNT tip, while the tube shapes come from the reaction with an imperfect CNT. The authors also mentioned that these carbides play a vital role in load transfer from the matrix to the reinforcement, since the fracture surfaces observed after tensile tests showed bridging and some broken CNTs without any CNT pulled out. This CNTs behavior is a consequence of their strong bonding to the metallic matrix. Zhou et al. [61] also studied the formation of these particles and their relationship with CNTs. These authors mention that the Al_4C_3 formed at the tip of MWCNTs can grow in the <100> direction of the CNTs, while those originated from nano defects can grow simultaneously in the <110> and <100> directions. An orientation relationship of Al(111)//CNT(002) was observed that means that the CNT reacted with the matrix and formed the carbine, which maintained the low-energy interface. The results confirmed that the Al_4C_3 contributes to the enhanced load transfer mechanism to the CNTs.

The increased dislocation density close to the CNTs and the Al_4C_3 can also assist the strengthening of the nanocomposites. The nanocomposites produced by powder metallurgy increase dislocations during the different steps of production caused by deformation. Previous works [5,45,52,53] already demonstrated that the CNT presence significantly affects the recovery, recrystallization, and grain growth during the sintering of Ni-CNT nanocomposites.

In Figure 12, it is possible to see HRTEM images and FFT of three different regions of the nanocomposites produced by ultrasonication: a region that corresponds to a CNT, a lattice of an Al_4C_3 particle, and an area with the presence of dislocation around the Al_4C_3 particle.

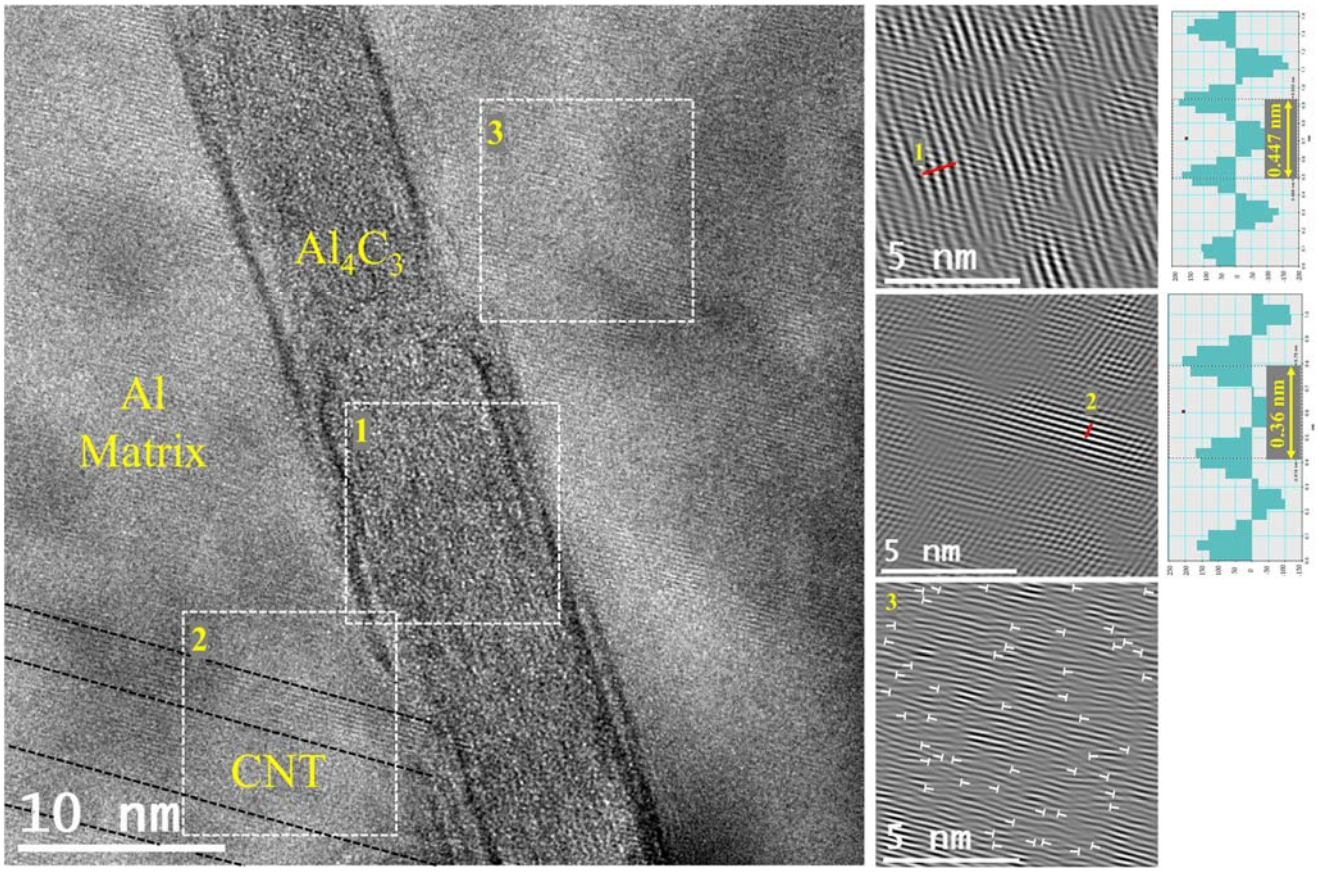

Figure 12. HRTEM image and inverse FFT showing the Al_4C_3, CNT embedded, and the presence of surrounding dislocations.

4. Conclusions

This work presents an overall view of the strengthening mechanisms of Al-CNT nanocomposites produced with 1.00 vol % CNTs. A classical powder metallurgy route was performed, using two different dispersion/mixture methods: ultrasonication and its combination with ball milling. This step of the production of nanocomposites is crucial to the dispersion of CNTs, ensuring its efficiency while obtaining a damage-free CNT structure so that the strengthening effect occurs. In this sense, the uniform dispersion of the CNTs with minimal damage is the key to improving the mechanical properties of the nanocomposites.

The mentioned improvement is a consequence of several strengthening mechanisms simultaneously, which are influenced by the presence of CNTs. The load transfer mechanism seems to contribute the most to the increase in the mechanical properties of the nanocomposites. The fracture surface showing pull-out and fractured CNTs confirms the critical role of this mechanism.

Strain hardening and second-phase hardening are also identified, since the formation of nanometric Al_4C_3 particles was observed together with a slight increase in dislocation density. Regarding grain size and texture hardening, as no significant differences were detected between the nanocomposites and the matrix, it was impossible to confirm their contributions to the Al-CNTs strengthening produced under these conditions.

Author Contributions: Conceptualization, Í.C.; investigation, Í.C. and S.S.; writing—original draft preparation, Í.C. and S.S.; supervision, S.S. and J.V.F.; formal analysis, S.S.; validation, S.S.; writing—review and editing S.S. and J.V.F. All authors have read and agreed to the published version of the manuscript.

Funding: Íris Carneiro: was supported by a Ph.D. grant for scientific research from the Portuguese Foundation for Science and Technology (FCT), with the reference PD/BD/143030/2018, and the P2020|Norte2020 program with the reference NORTE-08-5369-FSE-000051. This research was also supported by FEDER funds through the program COMPETE —Programa Operacional Factores de Competitividade, and by national funds through FCT—Fundação para a Ciência e a Tecnologia, under the project UIDB/EMS/00285/2020.

Institutional Review Board Statement: Not applicable.

Informed Consent Statement: Not applicable.

Data Availability Statement: Data can be available upon request from the authors.

Acknowledgments: The authors are grateful to CEMUP—Centro de Materiais da Universidade do Porto for expert assistance with SEM.

Conflicts of Interest: The authors declare no conflict of interest.

References

1. Suárez, S.; Reinert, L.; Mücklich, F. Carbon Nanotube (CNT)-Reinforced Metal Matrix Bulk Composites: MANUFACTURING and Evaluation. In *Diamond and Carbon Composites and Nanocomposites*; Aliofkhazraei, M., Ed.; InTech: Rijeka, Croatia, 2016; p. 129, ISBN: 978-953-512-454-2.
2. Agarwal, A.; Bakshi, S.R.; Lahiri, D. *Carbon Nanotubes: Reinforced Metal Matrix Composites*; CRC Press: Boca Raton, FL, USA, 2011; ISBN: 978-143-981-150-4.
3. Malaki, M.; Xu, W.; Kasar, A.K.; Menezes, P.L.; Dieringa, H.; Varma, R.S.; Gupta, M. Advanced Metal Matrix Nanocomposites. *Metals* **2019**, *9*, 330, https://doi.org/10.3390/met9030330.
4. Ashby, M.F.; Ferreira, P.J.; Schodek, D.L. Chapter 7—Nanomaterials: Properties. In *Nanomaterials, Nanotechnologies and Design*; Ashby, M.F., Ferreira, P.J., Schodek, D.L., Eds.; Butterworth-Heinemann: Boston, MA, USA, 2009; pp. 199–255, ISBN: 978-008-094-153-0.
5. Simões, S.; Carneiro, Í.; Viana, F.; Reis, M.A.L.; Vieira, M.F. Microstructural Characterization of Carbon Nanotubes (CNTs)-Reinforced Nickel Matrix Nanocomposites. *Microsc. Microanal.* **2019**, *25*, 180–186, https://doi.org/10.1017/S1431927618015064.
6. Suárez, S.; Ramos-Moore, E.; Lechthaler, B.; Mücklich, F. Grain growth analysis of multiwalled carbon nanotube-reinforced bulk Ni composites. *Carbon* **2014**, *70*, 173–178, https://doi.org/10.1016/j.carbon.2013.12.089.
7. Katzensteiner, A.; Müller, T.; Kormout, K.; Aristizabal, K.; Suarez, S.; Pippan, R.; Bachmaier, A. Influence of Processing Parameters on the Mechanical Properties of HPT-Deformed Nickel/Carbon Nanotube Composites. *Adv. Eng. Mater.* **2019**, *21*, 1800422, https://doi.org/10.1002/adem.201800422.
8. Singh, A.R.P.; Hwang, J.Y.; Scharf, T.W.; Tiley, J.; Banerjee, R. Bulk nickel–carbon nanotube nanocomposites by laser deposition. *Mater. Sci. Technol.* **2010**, *26*, 1393–1400, https://doi.org/10.1179/174328409X411899.
9. Wen, T.; Fan, K.; Zhang, F. High strength and high ductility in nickel matrix nanocomposites reinforced by carbon nanotubes and onion-like-carbon hybrid reinforcements. *J. Alloys Compd.* **2020**, *814*, 152303, https://doi.org/10.1016/j.jallcom.2019.152303.
10. Suárez, S.; Lasserre, F.; Mücklich, F. Mechanical properties of MWNT/Ni bulk composites: Influence of the microstructural refinement on the hardness. *Mater. Sci. Eng. A* **2013**, *587*, 381–386, https://doi.org/10.1016/j.msea.2013.08.058.
11. An, Z.; He, L.; Toda, M.; Yamamoto, G.; Hashida, T.; Ono, T. Microstructuring of carbon nanotubes-nickel nanocomposite. *Nanotechnology* **2015**, *26*, 195601, https://doi.org/10.1088/0957-4484/26/19/195601.
12. Faria, B.; Guarda, C.; Silvestre, N.; Lopes, J.N.C.; Galhofo, D. Strength and failure mechanisms of cnt-reinforced copper nanocomposite. *Compos. Part B Eng.* **2018**, *145*, 108–120, https://doi.org/10.1016/j.compositesb.2018.02.033.
13. Nayan, N.; Shukla, A.K.; Chandran, P.; Bakshi, S.R.; Murty, S.V.S.N.; Pant, B.; Venkitakrishnan, P.V. Processing and characterization of spark plasma sintered copper/carbon nanotube composites. *Mater. Sci. Eng. A* **2017**, *682*, 229–237, https://doi.org/10.1016/j.msea.2016.10.114.
14. Guiderdoni, C.; Pavlenko, E.; Turq, V.; Weibel, A.; Puech, P.; Estournès, C.; Peigney, A.; Bacsa, W.; Laurent, C. The preparation of carbon nanotube (CNT)/copper composites and the effect of the number of CNT walls on their hardness, friction and wear properties. *Carbon* **2013**, *58*, 185–197, https://doi.org/10.1016/j.carbon.2013.02.049.
15. Sule, R.; Olubambi, P.A.; Sigalas, I.; Asante, J.K.O.; Garrett, J.C. Effect of SPS consolidation parameters on submicron Cu and Cu–CNT composites for thermal management. *Powder Technol.* **2014**, *258*, 198–205, https://doi.org/10.1016/j.powtec.2014.03.034.
16. Li, H.; Misra, A.; Zhu, Y.; Horita, Z.; Koch, C.C.; Holesinger, T.G. Processing and characterization of nanostructured Cu-carbon nanotube composites. *Mater. Sci. Eng. A* **2009**, *523*, 60–64, https://doi.org/10.1016/j.msea.2009.05.031.
17. Pham, V.T.; Bui, H.T.; Tran, B.T.; Nguyen, V.T.; Le, D.Q.; Than, X.T.; Nguyen, V.C.; Doan, D.P.; Phan, N.M. The effect of sintering temperature on the mechanical properties of a Cu/CNT nanocomposite prepared via a powder metallurgy method. *Adv. Nat. Sci. Nanosci. Nanotechnol.* **2011**, *2*, 015006, https://doi.org/10.1088/2043-6262/2/1/015006.
18. Li, F.X.; Hao, P.D.; Yi, J.H.; Chen, Z.; Prashanth, K.G.; Maity, T.; Eckert, J. Microstructure and strength of nano-/ultrafine-grained carbon nanotube-reinforced titanium composites processed by high-pressure torsion. *Mater. Sci. Eng. A* **2018**, *722*, 122–128, https://doi.org/10.1016/j.msea.2018.03.007.

19. Munir, K.S.; Zheng, Y.; Zhang, D.; Lin, J.; Li, Y.; Wen, C. Improving the strengthening efficiency of carbon nanotubes in titanium metal matrix composites. *Mater. Sci. Eng. A* **2017**, *696*, 10–25, https://doi.org/10.1016/j.msea.2017.04.026.
20. Xue, F.; Jiehe, S.; Yan, F.; Wei, C. Preparation and elevated temperature compressive properties of multi-walled carbon nanotube reinforced Ti composites. *Mater. Sci. Eng. A* **2010**, *527*, 1586–1589, https://doi.org/10.1016/j.msea.2009.12.003.
21. Kondoh, K.; Threrujirapapong, T.; Umeda, J.; Fugetsu, B. High-temperature properties of extruded titanium composites fabricated from carbon nanotubes coated titanium powder by spark plasma sintering and hot extrusion. *Compos. Sci. Technol.* **2012**, *72*, 1291–1297, https://doi.org/10.1016/j.compscitech.2012.05.002.
22. Li, S.; Sun, B.; Imai, H.; Mimoto, T.; Kondoh, K. Powder metallurgy titanium metal matrix composites reinforced with carbon nanotubes and graphite. *Compos. A Appl. Sci. Manuf.* **2013**, *48*, 57–66, https://doi.org/10.1016/j.compositesa.2012.12.005.
23. Wang, F.-C.; Zhang, Z.-H.; Sun, Y.-J.; Liu, Y.; Hu, Z.-Y.; Wang, H.; Korznikov, A.V.; Korznikova, E.; Liu, Z.-F.; Osamu, S. Rapid and low temperature spark plasma sintering synthesis of novel carbon nanotube reinforced titanium matrix composites. *Carbon* **2015**, *95*, 396–407, https://doi.org/10.1016/j.carbon.2015.08.061.
24. Saikrishna, N.; Reddy, G.P.K.; Munirathinam, B.; Dumpala, R.; Jagannatham, M.; Sunil, B.R. An investigation on the hardness and corrosion behavior of MWCNT/Mg composites and grain refined Mg. *J. Magnes. Alloy.* **2018**, *6*, 83–89, https://doi.org/10.1016/j.jma.2017.12.003.
25. Shi, H.L.; Wang, X.J.; Zhang, C.L.; Li, C.D.; Ding, C.; Wu, K.; Hu, X.S. A Novel Melt Processing for Mg Matrix Composites Reinforced by Multiwalled Carbon Nanotubes. *J. Mater. Sci. Technol.* **2016**, *32*, 1303–1308, https://doi.org/10.1016/j.jmst.2016.05.014.
26. Goh, C.S.; Wei, J.; Lee, L.C.; Gupta, M. Ductility improvement and fatigue studies in Mg-CNT nanocomposites. *Compos. Sci. Technol.* **2008**, *68*, 1432–1439, https://doi.org/10.1016/j.compscitech.2007.10.057.
27. Aung, N.N.; Zhou, W.; Goh, C.S.; Nai, S.M.L.; Wei, J. Effect of carbon nanotubes on corrosion of Mg–CNT composites. *Corros. Sci.* **2010**, *52*, 1551–1553, https://doi.org/10.1016/j.corsci.2010.02.025.
28. Han, G.Q.; Shen, J.H.; Ye, X.X.; Chen, B.; Imai, H.; Kondoh, K.; Du, W.B. The influence of CNTs on the microstructure and ductility of CNT/Mg composites. *Mater. Lett.* **2016**, *181*, 300–304, https://doi.org/10.1016/j.matlet.2016.06.021.
29. Ding, Y.; Xu, J.; Hu, J.; Gao, Q.; Guo, X.; Zhang, R.; An, L. High performance carbon nanotube-reinforced magnesium nanocomposite. *Mater. Sci. Eng. A* **2020**, *771*, 138575, https://doi.org/10.1016/j.msea.2019.138575.
30. Simões, S.; Viana, F.; Reis, M.A.L.; Vieira, M.F. Aluminum and Nickel Matrix Composites Reinforced by CNTs: Dispersion/Mixture by Ultrasonication. *Metals* **2017**, *7*, 279, https://doi.org/10.3390/met7070279.
31. Chen, B.; Kondoh, K. Sintering Behaviors of Carbon Nanotubes—Aluminum Composite Powders. *Metals* **2016**, *6*, 213, doi: 10.3390/met6090213.
32. Simões, S.; Viana, F.; Reis, M.A.L.; Vieira, M.F. Microstructural Characterization of Aluminum-Carbon Nanotube Nanocomposites Produced Using Different Dispersion Methods. *Microsc. Microanal.* **2016**, *22*, 725–732, https://doi.org/10.1017/S143192761600057X.
33. Hassanzadeh-Aghdam, M.K.; Mahmoodi, M.J. A comprehensive analysis of mechanical characteristics of carbon nanotube-metal matrix nanocomposites. *Mater. Sci. Eng. A* **2017**, *701*, 34–44, https://doi.org/10.1016/j.msea.2017.06.066.
34. Singh, L.K.; Bhadauria, A.; Laha, T. Al-MWCNT nanocomposite synthesized via spark plasma sintering: Effect of powder milling and reinforcement addition on sintering kinetics and mechanical properties. *J. Mater. Res. Technol.* **2019**, *8*, 503–512, https://doi.org/10.1016/j.jmrt.2018.03.005.
35. Carvalho, O.; Miranda, G.; Soares, D.; Silva, F.S. Carbon nanotube dispersion in aluminum matrix composites—Quantification and influence on strength. *Mech. Adv. Mater. Struct.* **2016**, *23*, 66–73, https://doi.org/10.1080/15376494.2014.929766.
36. Xu, Z.Y.; Li, C.J.; Li, K.R.; Yi, J.H.; Tang, J.J.; Zhang, Q.X.; Liu, X.Q.; Bao, R.; Li, X. Carbon nanotube-reinforced aluminum matrix composites enhanced by grain refinement and in situ precipitation. *J. Mater. Sci.* **2019**, *54*, 8655–8664, https://doi.org/10.1007/s10853-019-03411-0.
37. Yu, Z.; Tan, Z.; Xu, R.; Ji, G.; Fan, G.; Xiong, D.-B.; Guo, Q.; Li, Z.; Zhang, D. Enhanced load transfer by designing mechanical interfacial bonding in carbon nanotube reinforced aluminum composites. *Carbon* **2019**, *146*, 155–161, https://doi.org/10.1016/j.carbon.2019.01.108.
38. Shahrdami, L.; Sedghi, A.; Shaeri, M.H. Microstructure and mechanical properties of Al matrix nanocomposites reinforced by different amounts of CNT and SiCW. *Compos. B Eng.* **2019**, *175*, 107081, https://doi.org/10.1016/j.compositesb.2019.107081.
39. Liu, Z.Y.; Xu, S.J.; Xiao, B.L.; Xue, P.; Wang, W.G.; Ma, Z.Y. Effect of ball-milling time on mechanical properties of carbon nanotubes reinforced aluminum matrix composites. *Compos. A Appl. Sci. Manuf.* **2012**, *43*, 2161–2168, https://doi.org/10.1016/j.compositesa.2012.07.026.
40. Jargalsaikhan, B.; Bor, A.; Lee, J.; Choi, H. Al/CNT nanocomposite fabrication on the different property of raw material using a planetary ball mill. *Adv. Powder Technol.* **2020**, *31*, 1957–1962, https://doi.org/10.1016/j.apt.2020.02.031.
41. Seo, H.Y.; Jiang, L.R.; Kang, C.G.; Jin, C.K. A Hot Extrusion Process without Sintering by Applying MWCNTs/Al6061 Composites. *Metals* **2018**, *8*, 184, https://doi.org/10.1016/j.msea.2017.04.041.
42. Cai, W.; Feng, X.; Sui, J. Preparation of multi-walled carbon nanotube-reinforced TiNi matrix composites from elemental powders by spark plasma sintering. *Rare Met.* **2012**, *31*, 48–50, https://doi.org/10.1007/s12598-012-0461-3.
43. Zhu, K.; Li, Z.; Jiang, C. Surface mechanical properties of shot-peened CNT/Al–Mg–Si alloy composites. *J. Alloys Compd.* **2019**, *773*, 1048–1053, https://doi.org/10.1016/j.jallcom.2018.09.165.

44. Chen, M.; Fan, G.; Tan, Z.; Yuan, C.; Xiong, D.; Guo, Q.; Su, Y.; Naito, M.; Li, Z. Tailoring and characterization of carbon nanotube dispersity in CNT/6061Al composites. *Mater. Sci. Eng. A* **2019**, *757*, 172–181, https://doi.org/10.1016/j.msea.2019.04.093.
45. Carneiro, Í.; Viana, F.; Vieira, F.M.; Fernandes, V.J.; Simões, S. EBSD Analysis of Metal Matrix Nanocomposite Microstructure Produced by Powder Metallurgy. *Nanomaterials* **2019**, *9*, 878, https://doi.org/10.3390/nano9060878.
46. Chen, B.; Shen, J.; Ye, X.; Jia, L.; Li, S.; Umeda, J.; Takahashi, M.; Kondoh, K. Length effect of carbon nanotubes on the strengthening mechanisms in metal matrix composites. *Acta Mater.* **2017**, *140*, 317–325, https://doi.org/10.1016/j.actamat.2017.08.048.
47. Han, T.; Wang, F.; Li, J.; Zhao, N.; He, C. Simultaneously enhanced strength and ductility of Al matrix composites through the introduction of intragranular nano-sized graphene nanoplates. *Compos. B. Eng.* **2021**, *212*, 108700, https://doi.org/10.1016/j.compositesb.2021.108700.
48. Kwon, H.; Park, D.H.; Silvain, J.F.; Kawasaki, A. Investigation of carbon nanotube reinforced aluminum matrix composite materials. *Compos. Sci. Technol.* **2010**, *70*, 546–550, https://doi.org/10.1016/j.compscitech.2009.11.025.
49. Chen, B.; Kondoh, K.; Umeda, J.; Li, S.; Jia, L.; Li, J. Interfacial in-situ Al2O3 nanoparticles enhance load transfer in carbon nanotube (CNT)-reinforced aluminum matrix composites. *J. Alloys Compd.* **2019**, *789*, 25–29, https://doi.org/10.1016/j.jallcom.2019.03.063.
50. Chen, B.; Kondoh, K.; Li, J.S. In-situ observation of interaction between dislocations and carbon nanotubes in aluminum at elevated temperatures. *Mate. Lett.* **2020**, *264*, 127323, https://doi.org/10.1016/j.matlet.2020.127323.
51. Simões, S.; Viana, F.; Reis, M.A.L.; Vieira, M.F. Improved dispersion of carbon nanotubes in aluminum nanocomposites. *Compos. Struct.* **2014**, *108*, 992–1000, https://doi.org/10.1016/j.compstruct.2013.10.043.
52. Carneiro, Í.; Simões, S. Effect of Morphology and Structure of MWCNTs on Metal Matrix Nanocomposites. *Materials* **2020**, *13*, 5557, https://doi.org/10.3390/ma13235557.
53. Carneiro, Í.; Fernandes, J.V.; Simões, S. Investigation on the Strengthening Mechanisms of Nickel Matrix Nanocomposites. *Nanomaterials* **2021**, *11*, 1426, https://doi.org/10.3390/nano11061426.
54. Beausir, B.; Fundenberger, J.-J. Analysis Tools for Electron and X-ray diffraction, ATEX—Software; Université de Lorraine—Metz. 2017. Available online: www.atex-software.eu (accessed on 11 June 2021).
55. Zhang, X.; Li, S.; Pan, B.; Pan, D.; Zhou, S.; Yang, S.; Jia, L.; Kondoh, K. A novel strengthening effect of in-situ nano Al2O3w on CNTs reinforced aluminum matrix nanocomposites and the matched strengthening mechanisms. *J. Alloys Compd.* **2018**, *764*, 279–288, https://doi.org/10.1016/j.jallcom.2018.06.006.
56. Xiong, N.; Bao, R.; Yi, J.; Fang, D.; Tao, J.; Liu, Y. CNTs/Cu-Ti composites fabrication through the synergistic reinforcement of CNTs and in situ generated nano-TiC particles. *J. Alloy. Compd.* **2019**, *770*, 204–213, https://doi.org/10.1016/j.jallcom.2018.08.116.
57. Yoo, S.; Han, S.; Kim, W. A combination of ball milling and high-ratio differential speed rolling for synthesizing carbon nanotube/copper composites. *Carbon* **2013**, *61*, 487–500, https://doi.org/10.1016/j.carbon.2013.04.105.
58. Chen, B.; Shen, J.; Ye, X.; Imai, H.; Umeda, J.; Takahashi, M.; Kondoh, K. Solid-state interfacial reaction and load transfer efficiency in carbon nanotubes (CNTs)-reinforced aluminum matrix composites. *Carbon* **2017**, *114*, 198–208, https://doi.org/10.1016/j.carbon.2016.12.013.
59. Chen, B.; Jia, L.; Li, S.; Imai, H.; Takahashi, M.; Kondoh, K. In Situ Synthesized Al4C3 Nanorods with Excellent Strengthening Effect in Aluminum Matrix Composites. *Adv. Eng. Mater.* **2014**, *16*, 972–975, https://doi.org/10.1002/adem.201400232.
60. Zhou, W.; Yamaguchi, T.; Kikuchi, K.; Nomura, N.; Kawasaki, A. Effectively enhanced load transfer by interfacial reactions in multi-walled carbon nanotube reinforced Al matrix composites. *Acta Mater.* **2017**, *125*, 369–376, https://doi.org/10.1016/j.actamat.2016.12.022.
61. Zhou, W.; Bang, S.; Kurita, H.; Miyazaki, T.; Fan, Y.; Kawasaki, A. Interface and interfacial reactions in multi-walled carbon nanotube-reinforced aluminum matrix composites. *Carbon* **2016**, *96*, 919–928, https://doi.org/10.1016/j.carbon.2015.10.016.